Supporting Information

Efficient Heteronuclear Diatom Electrocatalyst for Nitrogen Reduction Reaction: Pd–Nb Diatom Supported on Black Phosphorus

*Zeyun Zhang, and Xuefei Xu**

Center for Combustion Energy, Department of Energy and Power Engineering, Key Laboratory for Thermal Science and Power Engineering of Ministry of Education, and Beijing Key Laboratory of CO_2 Utilization and Reduction Technology, Tsinghua University, Beijing 100084, China

E-mail: xuxuefei@tsinghua.edu.cn

Contents

1. Two N_2 adsorption patterns on M@BP

(a) **(b)**

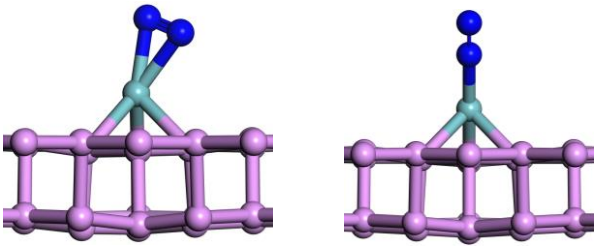

Figure S1. N_2 adsorption on M@BP via (a) side-on and (b) end-on patterns. P, pink; N, blue; M, dark green.

2. Optimized structures of PdNb@BP, Pd_2Nb@BP, and $PdNb_2$@BP

(a)

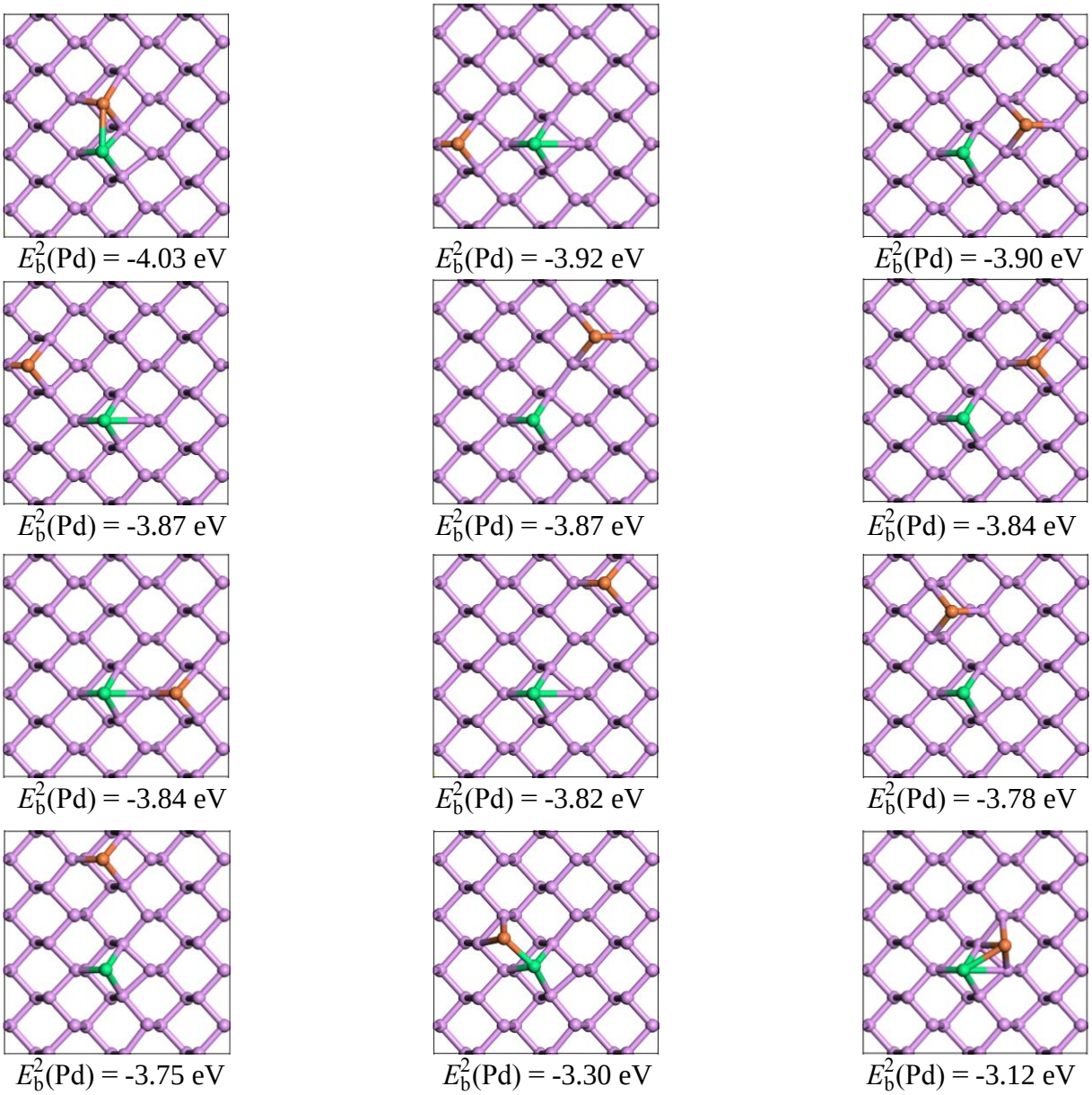

(b)

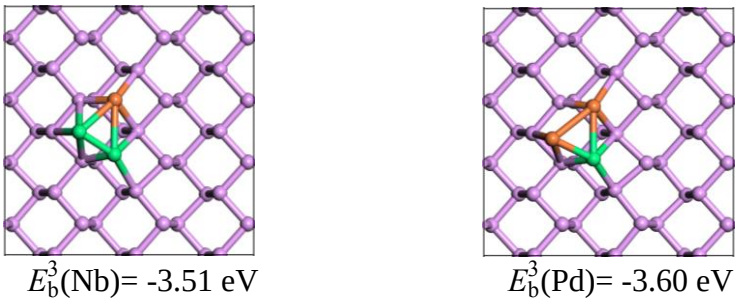

Figure S2. (a) the optimized structures of PdNb@BP and the corresponding binding energies of Pd supported on Nb@BP; (b) the optimized structures of Pd_2Nb@BP and $PdNb_2$@BP, and the corresponding binding energies of Nb and Pd supported on PdNb@BP. P, pink; Nb, green and Pd, orange.

3. AIMD simulation of PdNb@BP in vacuum

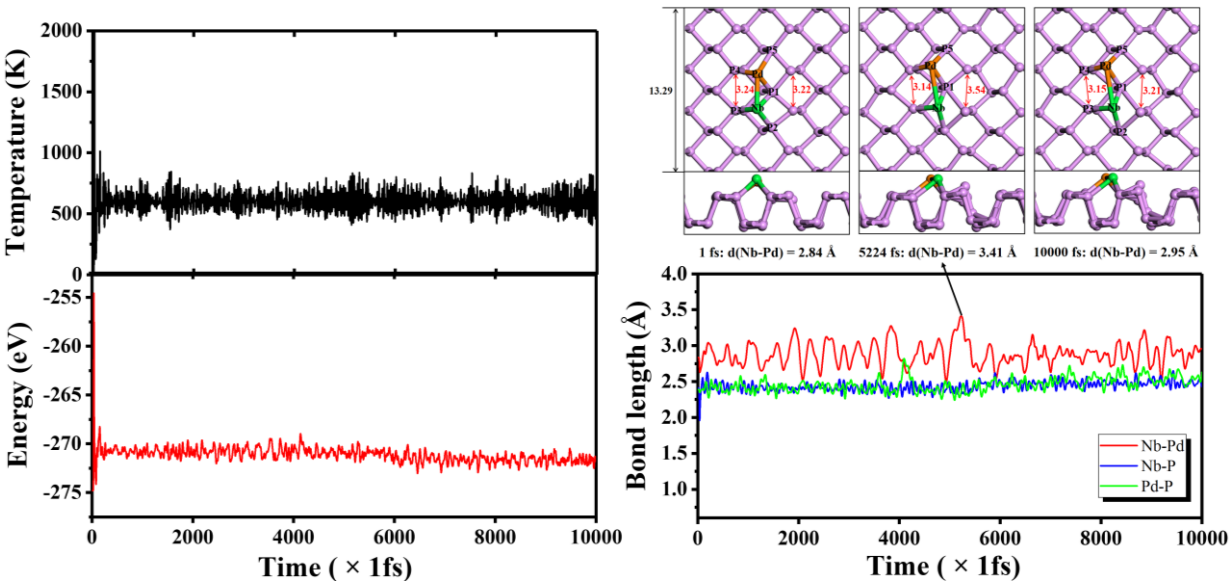

Figure S3. Variations of temperature, energy and key bond lengths against time for AIMD simulation of PdNb@BP at 600 K, and the top and side views of three representative snapshots (at 1 fs, 5224 fs, and 10000 fs, respectively) of the atomic configurations. The simulation was run for 10 ps with a time step of 1 fs. Bond lengths are given in Å. The bond length of Nb-P is the average bond length of Nb-P1, Nb-P2, and Nb-P3 bonds; the bond length of Pd-P is the average bond length of Pd-P1, Pd-P4, and Nb-P5 bonds. P, pink; Nb, green and Pd, orange.

4. AIMD simulation of PdNb@BP under aqueous environment

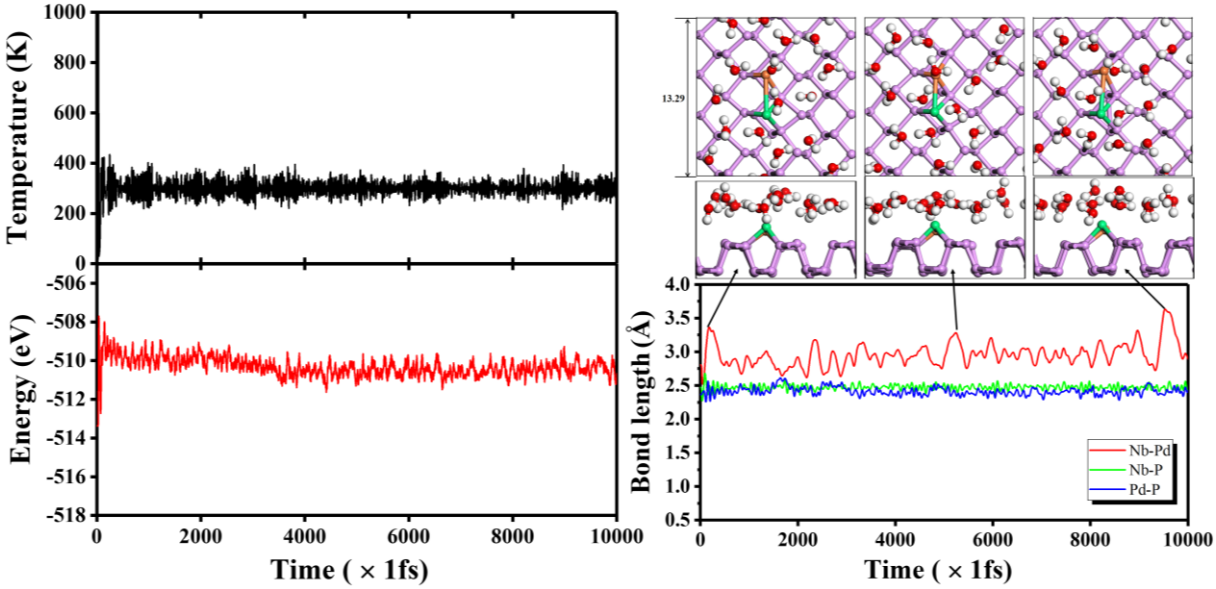

Figure S4. Variations of temperature, energy and key bond lengths against time for AIMD simulation of PdNb@BP with one-layer water molecules at 300 K, and the top and side views of three representative snapshots (at 182 fs, 4623 fs, and 9532 fs, respectively) of the atomic configurations. P, pink; Nb, green; Pd, orange; O, red and H, white. Here we use one-layer water molecules over the catalyst surface to simulate the aqueous environment.

5. N_2 adsorbed structures (B3 and B4) on PdNb@BP

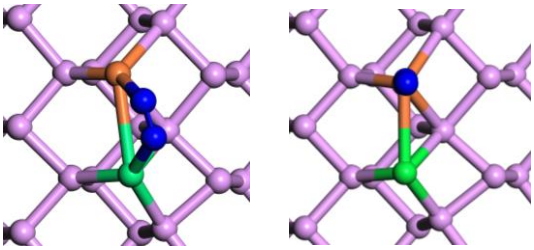

B3 **B4**

Figure S5. The optimized **B3** and **B4** structures for N_2 adsorption on PdNb@BP. P, pink; Nb, green; Pd, orange; N, blue.

6. The transfer of NH_3 from Nb site to Pd site with the help of an additional N_2 molecule

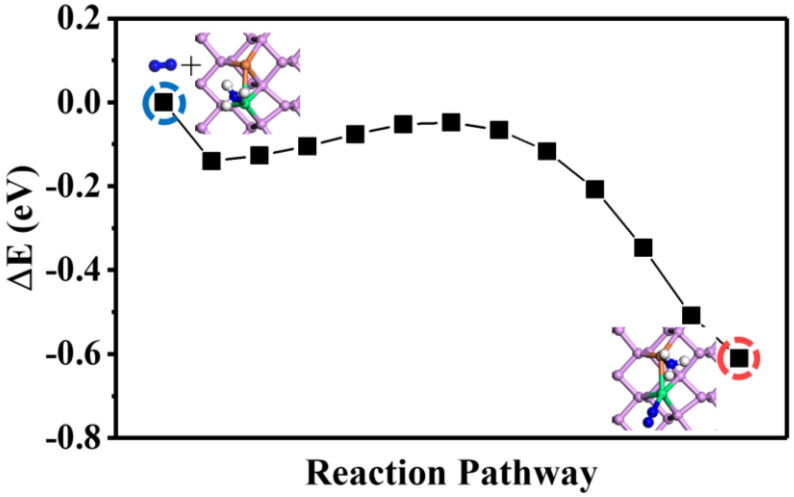

Figure S6. Energy evolution profile for transfer of NH_3 from Nb site to Pd site with the help of an additional N_2 molecule. P, pink; Nb, green; Pd, orange; N, blue; H, white. The potential energy surface was scanned along linearly interpolated reaction coordinates, and for each interpolated structure, one N atom of N_2, the N atom of NH_3, and the Nb atom were fixed, while all other degrees of freedom were optimized.

7. Free-energy diagrams of eNRR and HER on PdNb@BP at different applied electrode potentials

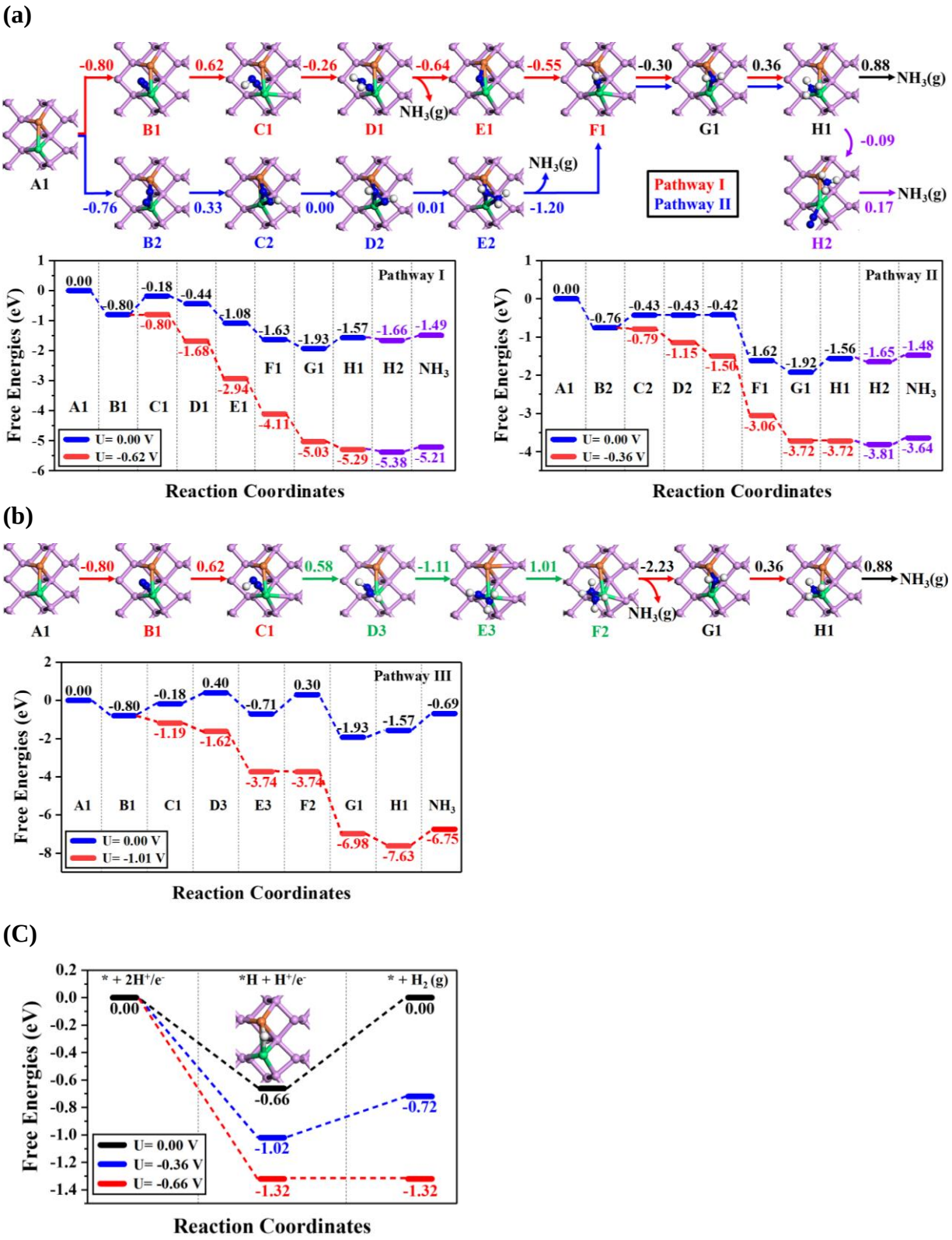

Figure S7. Free-energy profiles (in eV) of eNRR through (a) distal (Pathway **I**), enzymatic (pathway **II**), and (b) alternating (pathway **III**) mechanisms and of (c) HER on PdNb@BP at different applied electrode potentials. P, pink; Nb, green; Pd, orange; N, blue; H, white.

The limiting potentials of eNRR on PdNb@BP through pathways **I** and **II** are calculated as −0.62 V and −0.36 V according to $U_{limiting} = -\Delta G_{max}(U = 0)/e$, respectively. Similarly, the limiting potential of HER on PdNb@BP is -0.66 V. When an electrode potential U = -0.36 V ($U_{limiting}$ of pathway **II**) is applied, the hydrogenation steps of eNRR along pathway **II** are all downhill, but the pathway **I** of eNRR and the HER reaction are still uphill in energy. However, N_2 activation is a thermodynamic process, while H adsorption is a electrochemical process and can be stablized by the applied electrode potential. At zero electrode potential (U = 0 V), the N_2 adsorption is more favorable than H adsorption. When U < -0.1 V, the H adsorption starts to be more competitive with N_2 adsorption with increasing $|U|$, which will lower the eNRR efficiency. When U < -0.66 V, the HER occurs and further lowers the Faraday efficiency of eNRR.

8. Free-energy barriers of hydrogenation steps along the optimal pathway II

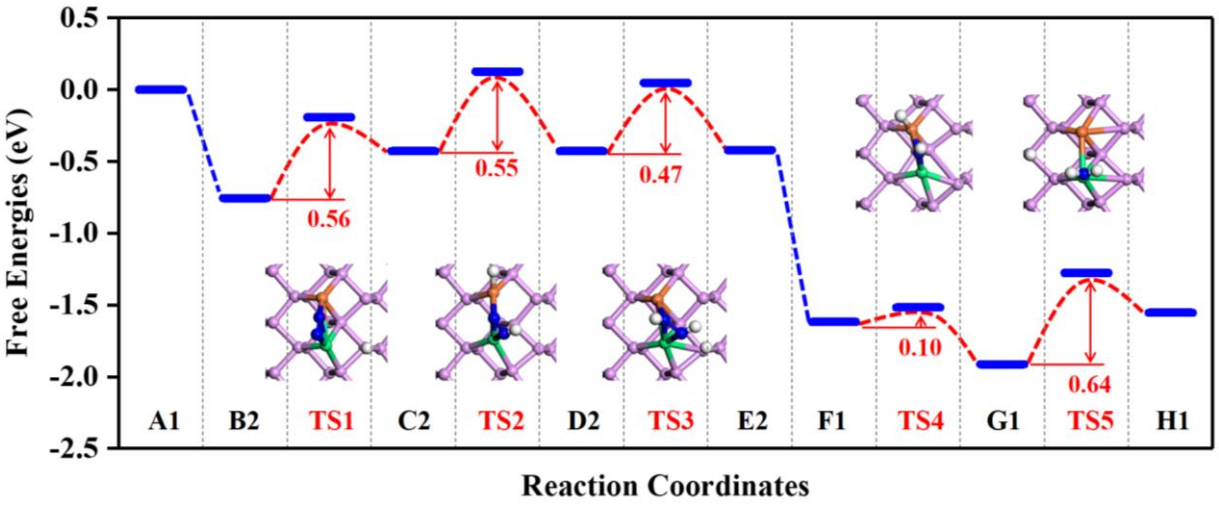

Figure S8. Free-energy profile of eNRR on PdNb@BP along pathway **II** at zero electrode potential. The inserted structures are the located transition states, and the numbers in red are the estimated activation barriers. P, pink; Nb, green; Pd, orange; N, blue; H, white; O, red.

We adopted the method proposed by Janik and his coworkers[1,2] to estimate the activation barrier of each electrochemical hydrogenation step (*A + H^+ + e^- → *AH) along the pathway **II**. This method is based on a resonable assumption that the electrocatalytic reduction is following an inner-sphere Marcurs mechanism. That is, the transition-state (TS) structure is assmued to be local to the adsorbed *A species, and the electron transfer is assumed to be rapid near the transition-state structure. At the equilibrium potential of the reductive adsorption of a proton, U^0, the TS of an analogous chemcial hydrogenation reaction (*A + *H → *AH) with the hydrogen pre-adsorbed on the catalyst surface near the adsorbed *A is assumed to be equivalent to that of the electrochemical hydrogenation step. Thus, instead of direct location of the TS for the electrochemical hydrogenation step, one can search for a TS of the chemcial hydrogenation reaction. Then, the activation barrier of the electrochemical hydrogenation step at an applied electrode potential U, $\Delta G_{act}(U)$, is calculated by

$$\Delta G_{act}(U) = \Delta G_{act}^{DFT}(U^0) + \beta(eU - eU^0) \quad \text{(S1)}$$

where $\Delta G_{act}^{DFT}(U^0)$ is the free-energy difference between the located transition state and the reactant state (*A + H^+ + e^-) obtained from DFT calculations, and β is the symmetry coefficient, which was approximately set to 0.5 for all elementary reaction steps in this work. **Figure S8** shows the free energy profile of eNRR on PdNb@BP along pathway **II** calculated at zero electrode potential.

At zero electrode potential, activation free energy barriers of 0.56, 0.55, and 0.47 eV are estamated for the first three hydrogenation steps, respectively. The first ammonia formation is an energy-favorable process without passing through a transition state. The hydrogenation step from *NH to *NH_2 needs a very small activation barrier of 0.10 eV. The highest barrier of the eNRR process on PdNb@BP occurs at the sixth hydrogenation step from *NH_2 to *NH_3 (**G1→H1**, 0.64 eV), and theorefore this step is identified as the rate-determining step. This is in good aggreement with our prediction from the perspective of thermodynamics.

9. NH_3 desorption free energy from Nb_2@BP with or without the aid of additional N_2 molecule

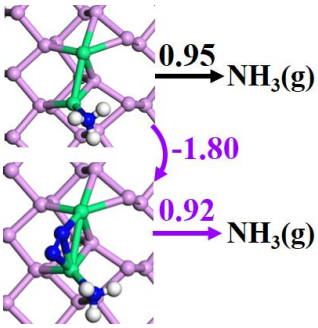

Figure S9. Free-energy changes (in eV) of NH_3 desorption from Nb_2@BP with or without the aid of additional N_2 adorption and the corresponding structures. P, pink; Nb, green; Pd, orange; N, blue; H, white.

10. The projected density of state (PDOS) profiles of N_2 adsorption on PdNb@BP (B1 and B3)

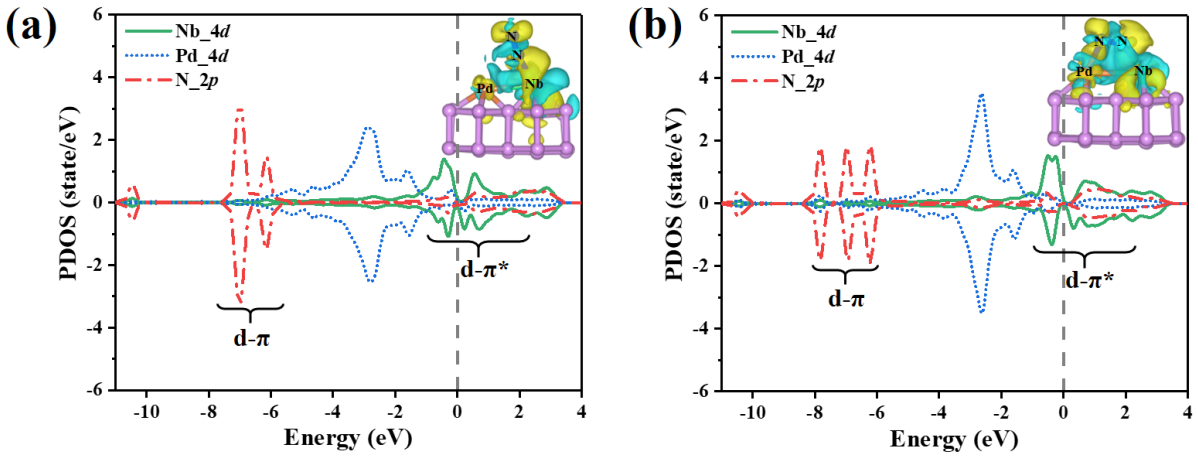

Figure S10. The projected density of state (PDOS) profiles of Nb 4d, Pd 4d and N 2p orbitals after N_2 adsorption on PdNb@BP: (a) **B1** and (b) **B3**. The Fermi energy level is set to zero and indicated by the vertical dashed line. The inserted figures show the charge density change after N_2 adsorption on PdNb@BP. The positive and negative charges are shown in yellow and cyan, respectively. P, pink; Nb, green; Pd, orange; N, blue.

11. The free energy changes of the first and the sixth hydrogenation steps and the desorption free energy of NH_3 on M@BP

Table S1. The free energy changes (in eV) of the first and the sixth hydrogenation steps and the desorption free energy (in eV) of NH_3 on M@BP

M	$\Delta G_{N_2\text{-}N_2H}$ (side-on)	$\Delta G_{N_2\text{-}N_2H}$ (end-on)	$\Delta G_{NH_2\text{-}NH_3}$	$\Delta G_{des\text{-}NH_3}$
Sc	0.52	2.03	0.47	0.86
Ti	0.44	1.86	0.39	0.93
V	0.46	0.78	0.36	1.08
Fe	0.84	0.88	-0.45	0.96
Co	1.04	1.20	-0.65	0.89
Ni	1.69	1.78	-1.04	0.74
Nb	0.37	0.98	0.25	0.84
Mo	0.87	0.69	-0.12	1.31
Tc	0.55	0.99	0.16	0.90
Ru	0.92	0.88	-0.33	0.78
Rh	1.22	1.10	-0.70	0.55
Pd	1.87	1.89	-1.32	0.36
Ta	0.18	0.69	0.62	1.03
W	0.45	0.47	0.28	1.59
Re	0.33	0.46	0.60	1.14
Os	0.82	0.59	0.23	0.97
Pt	1.65	1.74	-0.87	0.53

12. Comparison of the eNRR performances of PdNb@BP with those of ever-reported catalysts

Table S2. Comparison of the Gibbs free energy changes of the rate-determining step and NH_3 desorption of PdNb@BP with those of some ever-reported catalysts.

catalyst	rate-determining step	ΔG_{rds} (eV)	$\Delta G_{des\text{-}NH_3}$ (eV)
edge BP[3]	*NN-*NNH	0.85	0.70
doubly B-doped BP[4]	*N*N-*N*NH	0.19	-[a]
MoB_2-BP[5]	*NN-*NNH	0.60	0.66
Mo_1N_3-BP[6]	*NN-*NNH	0.18	0.56
V@BP[7]	*NH_2-*NH_3	0.34	0.31
Ru-doped BP[8]	*N*N-*N*NH	0.86	0.43
W@BP[9]	*NH_2*NH-*NH_2*NH_2	0.46	1.21
Mo-doped BN[10]	*NH_2-*NH_3	0.35	0.70
Fe-deposited MoS_2[11]	*NN-*NNH	0.99	0.56
B-doped C_2N[12]	*N*NH-*NH*NH	0.15	3.72
B/g-C_3N_4[13]	*NH_2*NH_2-*NH_2	0.20	1.79
W@N-doped graphyne[14]	*NN-*NNH	0.29	1.22
B-doped BN edge[15]	*NH-*NH_2	0.29	0.85
Mo_1-N_1C_2-graphene[16]	*N*N-*N*NH	0.40	0.47
Mn_2@g-C_2N[17]	*NH_2*NH-*NH_2*NH_2	0.23	-[a]
Mo_2@g-C_2N[18]	*NH-*NH_2	0.41	0.49
Co_2@GDY[19]	*NH_2-*NH_3	0.43	0.73
Ru_2-N_6@Graphene[20]	*NH_2-*NH_3	0.36	0.66
Mo-Ru-N_4@Graphene[21]	*N*N-*N*NH	0.17	0.41
FeV@C_2N[22]	*NNH-*NHNH	0.17	-[a]
This work	*NH_2-*NH_3	0.36	0.17

[a] The NH_3 desorption free energy was not reported.

13. The zero-point energies and entropies of key species

Table S3. Calculated zero-point energies and entropies of different adsorption species on M@BP and PdNb@BP. The *TS* is the entropy contribution to the free energy at 298.15 K.

Catalyst	side on *N*N		end on *NN		*N*NH	
M	E_{zpe} (eV)	*TS* (eV)	E_{zpe} (eV)	*TS* (eV)	E_{zpe} (eV)	*TS* (eV)
Sc	0.19	0.16	0.21	0.15	0.49	0.14
Ti	0.19	0.16	0.21	0.15	0.49	0.14
V	0.19	0.16	0.18	0.19	0.49	0.14
Cr	0.18	0.19	0.20	0.16	0.48	0.15
Mn	0.19	0.15	0.20	0.16	0.48	0.15
Fe	0.18	0.18	0.20	0.16	0.49	0.14
Co	0.18	0.18	0.21	0.16	0.46	0.15
Ni	0.19	0.17	0.21	0.15	0.44	0.17
Y	0.19	0.14	0.21	0.15	N/A	N/A
Zr	0.19	0.16	0.21	0.15	N/A	N/A
Nb	0.19	0.16	0.21	0.15	0.49	0.12
Mo	0.19	0.15	0.21	0.15	0.48	0.15
Tc	0.19	0.16	0.21	0.15	0.49	0.14
Ru	0.20	0.17	0.19	0.18	0.47	0.17
Rh	0.18	0.19	0.20	0.18	0.47	0.16
Pd	0.17	0.21	0.19	0.18	0.43	0.19
Lu	0.19	0.16	0.21	0.15	N/A	N/A
Hf	0.19	0.16	0.21	0.15	N/A	N/A
Ta	0.19	0.15	0.21	0.15	0.49	0.12
W	0.19	0.14	0.20	0.15	0.49	0.13
Re	0.19	0.14	0.21	0.14	0.49	0.14
Os	0.19	0.16	0.21	0.15	0.47	0.17
Ir	0.19	0.16	0.21	0.15	N/A	N/A
Pt	0.18	0.17	0.20	0.17	0.45	0.16

Catalyst	*NNH		*NH_2		*NH_3	
M	E_{zpe} (eV)	*TS* (eV)	E_{zpe} (eV)	*TS* (eV)	E_{zpe} (eV)	*TS* (eV)
Sc	0.48	0.16	0.65	0.13	1.02	0.16
Ti	0.48	0.16	0.65	0.13	1.03	0.16
V	0.45	0.19	0.65	0.14	1.01	0.19
Cr	0.46	0.18	0.66	0.14	1.01	0.19
Mn	0.48	0.16	0.66	0.12	1.03	0.16
Fe	0.48	0.16	0.67	0.12	1.03	0.16
Co	0.49	0.15	0.65	0.14	1.04	0.16
Ni	0.44	0.19	0.65	0.13	1.03	0.16
Y	N/A	N/A	N/A	N/A	N/A	N/A
Zr	N/A	N/A	N/A	N/A	N/A	N/A
Nb	0.48	0.14	0.65	0.12	1.02	0.15
Mo	0.48	0.17	0.65	0.13	1.02	0.16
Tc	0.48	0.14	0.65	0.13	1.02	0.16
Ru	0.48	0.16	0.67	0.11	1.03	0.15
Rh	0.48	0.16	0.67	0.12	1.02	0.18
Pd	0.42	0.22	0.65	0.13	1.02	0.17
Lu	N/A	N/A	N/A	N/A	N/A	N/A
Hf	N/A	N/A	N/A	N/A	N/A	N/A
Ta	0.48	0.16	0.65	0.13	1.02	0.16
W	0.50	0.14	0.65	0.14	1.02	0.16
Re	0.50	0.14	0.67	0.13	1.04	0.14
Os	0.48	0.16	0.67	0.11	1.03	0.15
Ir	N/A	N/A	N/A	N/A	N/A	N/A
Pt	0.46	0.17	0.65	0.14	1.03	0.17

	NbPd@BP			Nb@BP	
	E_{zpe} (eV)	*TS* (eV)		E_{zpe} (eV)	*TS* (eV)
B1	0.20	0.15	side on *N*N	0.19	0.16
B2	0.19	0.13	end on *NN	0.21	0.15
B3	0.19	0.13	*N*NH	0.49	0.12
B4	0.18	0.14	*NNH	0.48	0.14
C1	0.48	0.14	*NH*NH	0.79	0.15
C2	0.48	0.13	*NHNH	0.80	0.17
D1	0.81	0.18	*NNH_2	0.81	0.16
D2	0.74	0.13	*NH*NH_2	1.15	0.17
E1	0.09	0.04	*$NHNH_2$	1.03	0.13
E2	1.14	0.14	*N	0.08	0.06
F1	0.35	0.08	*NH_2*NH_2	1.36	0.18
G1	0.68	0.09	*NH_2NH_2	1.49	0.21
H1	1.02	0.15	*NH	0.36	0.08
H2	1.23	0.29	*NH_2	0.65	0.12
			*NH_3	1.02	0.15
			*NH_3*NN	1.23	0.31

References

[1] Rostamikia, G.; Mendoza, A. J.; Hickner, M. A.; Janik, M. J. First-Principles Based Microkinetic Modeling of Borohydride Oxidation on a Au(1 1 1) Electrode. *J. Pow. Sour.* **2011**, *196*, 9228-9237.

[2] Nie, X.; Esopi, M. R.; Janik, M. J.; Asthagiri, A. Selectivity of CO_2 Reduction on Copper Electrodes: The Role of the Kinetics of Elementary Steps. *Angew. Chem., Int. Ed. Engl.* **2013,** *52*, 2459-2462.

[3] Zhang, L.; Ding, L. X.; Chen, G. F.; Yang, X.; Wang, H. Ammonia Synthesis Under Ambient Conditions: Selective Electroreduction of Dinitrogen to Ammonia on Black Phosphorus Nanosheets. *Angew. Chem., Int. Ed. Engl.* **2019,** *58*, 2612-2616.

[4] Shi, L.; Li, Q.; Ling, C.; Zhang, Y.; Ouyang, Y.; Bai, X.; Wang, J. Metal-Free Electrocatalyst for Reducing Nitrogen to Ammonia Using a Lewis Acid Pair. *J. Mater. Chem. A* **2019,** *7*, 4865-4871.

[5] Li, Q.; Qiu, S.; Liu, C.; Liu, M.; He, L.; Zhang, X.; Sun, C. Computational Design of Single-Molybdenum Catalysts for the Nitrogen Reduction Reaction. *J. Phys. Chem. C* **2019,** *123*, 2347-2352.

[6] Ou, P.; Zhou, X.; Meng, F.; Chen, C.; Chen, Y.; Song, J. Single Molybdenum Center Supported on N-Doped Black Phosphorus as an Efficient Electrocatalyst for Nitrogen Fixation. *Nanoscale* **2019,** *11*, 13600-13611.

[7] Liang, X.; Deng, X.; Guo, C.; Wu, C.-M. L. Activity Origin and Design Principles for Atomic Vanadium Anchoring on Phosphorene Monolayer for Nitrogen Reduction Reaction. *Nano Res.* **2020,** *13*, 2925-2932.

[8] Liu, J.-D.; Wei, Z.-X.; Dou, Y.-H.; Feng, Y.-Z.; Ma, J.-M. Ru-Doped Phosphorene for Electrochemical Ammonia Synthesis. *Rare Met.* **2020,** *39*, 874-880.

[9] Liu, K.; Fu, J.; Zhu, L.; Zhang, X.; Li, H.; Liu, H.; Hu, J.; Liu, M. Single-Atom Transition Metals Supported on Black Phosphorene for Electrochemical Nitrogen Reduction. *Nanoscale* **2020,** *12*, 4903-4908.

[10] Zhao, J.; Chen, Z. Single Mo Atom Supported on Defective Boron Nitride Monolayer as an Efficient Electrocatalyst for Nitrogen Fixation: A Computational Study. *J. Am. Chem. Soc.* **2017,** *139*, 12480-12487.

[11] Azofra, L. M.; Sun, C.; Cavallo, L.; MacFarlane, D. R. Feasibility of N_2 Binding and Reduction to Ammonia on Fe- Deposited MoS_2 2D Sheets: A DFT Study. *Chem-Eur J.* **2017,** *23*, 8275-8279.

[12] Ji, S.; Wang, Z.; Zhao, J., A Boron-Interstitial Doped C_2N Layer as A Metal-Free Electrocatalyst for N_2 Fixation: A Computational Study. *J. Mater. Chem. A* **2019,** *7*, 2392-2399.

[13] Ling, C.; Niu, X.; Li, Q.; Du, A.; Wang, J., Metal-Free Single Atom Catalyst for N_2 Fixation Driven by Visible Light. *J. Am. Chem. Soc.* **2018,** *140*, 14161-14168.

[14] He, T.; Matta, S. K.; Du, A. Single Tungsten Atom Supported on N-Doped Graphyne as a High-Performance Electrocatalyst for Nitrogen Fixation under Ambient Conditions. *Phys. Chem. Chem. Phys.* **2019,** *21*, 1546-1551.

[15] Mao, X.; Zhou, S.; Yan, C.; Zhu, Z.; Du, A. A Single Boron Atom Doped Boron Nitride Edge as a Metal-Free Catalyst for N_2 Fixation. *Phys. Chem. Chem. Phys.* **2019,** *21*, 1110-1116.

[16] Ling, C.; Bai, X.; Ouyang, Y.; Du, A.; Wang, J. Single Molybdenum Atom Anchored on N-Doped Carbon as a Promising Electrocatalyst for Nitrogen Reduction into Ammonia at Ambient Conditions. *J. Phys. Chem. C* **2018,** *122*, 16842-16847.

[17] Chen, Z. W.; Yan, J. M.; Jiang, Q. Single or Double: Which is the Altar of Atomic Catalysts for Nitrogen Reduction Reaction? *Small Methods* **2018,** *3*, 1800291.

[18] Zhang, X.; Chen, A.; Zhang, Z.; Zhou, Z. Double-Atom Catalysts: Transition Metal Dimer-Anchored C_2N Monolayers as N_2 Fixation Electrocatalysts. *J. Mater. Chem. A* **2018,** *6*, 18599-18604.

[19] Ma, D.; Zeng, Z.; Liu, L.; Huang, X.; Jia, Y., Computational Evaluation of Electrocatalytic Nitrogen Reduction on TM Single-, Double-, and Triple-Atom Catalysts (TM = Mn, Fe, Co, Ni) Based on Graphdiyne Monolayers. *J. Phys. Chem. C* **2019,** *123*, 19066-19076.

[20] Deng, T.; Cen, C.; Shen, H.; Wang, S.; Guo, J.; Cai, S.; Deng, M. Atom-Pair Catalysts Supported by N-Doped Graphene for the Nitrogen Reduction Reaction: d-Band Center-Based Descriptor. *J. Phys. Chem. Lett.* **2020,** *11*, 6320-6329.

[21] He, T.; Puente Santiago, A. R.; Du, A. Atomically Embedded Asymmetrical Dual-Metal Dimers on N-Doped Graphene for Ultra-Efficient Nitrogen Reduction Reaction. *J. Catal.* **2020,** *388*, 77-83.

[22] Wei, Z.; He, J.; Yang, Y.; Xia, Z.; Feng, Y.; Ma, J. Fe, V-co-Doped C_2N for Electrocatalytic N_2-to-NH_3 Conversion. *J. Energy Chem.* **2021,** *53*, 303-308.